

1-18-2011

On the Importance of Band Gap Formation in Graphene for Analog Device Application

Saptarshi Das

Doctoral Student, sdas@purdue.edu

Joerg Appenzeller

Birck Nanotechnology Center, Purdue University

Follow this and additional works at: <http://docs.lib.purdue.edu/nanopub>

 Part of the [Electrical and Electronics Commons](#), [Electronic Devices and Semiconductor Manufacturing Commons](#), [Nanoscience and Nanotechnology Commons](#), and the [VLSI and Circuits, Embedded and Hardware Systems Commons](#)

Das, Saptarshi and Appenzeller, Joerg, "On the Importance of Band Gap Formation in Graphene for Analog Device Application" (2011). *Birck and NCN Publications*. Paper 780.

<http://dx.doi.org/10.1109/TNANO.2011.2109007>

This document has been made available through Purdue e-Pubs, a service of the Purdue University Libraries. Please contact epubs@purdue.edu for additional information.

On The Importance of Bandgap Formation in Graphene for Analog Device Applications

Saptarshi Das and Joerg Appenzeller, Fellow, IEEE

Dept of Electrical and Computer Engineering, Birck nanotechnology center, Purdue University

Abstract— We present a study that identifies the ideal bandgap value in graphene devices, e.g. through size quantization in graphene nano-ribbons, to enable graphene based high performance RF applications. When considering a ballistic graphene nano-ribbon low noise amplifier (GNR-LNA), including aspects like stability, gain, power dissipation and load impedance, our calculations predict a finite bandgap of the order of $E_g \approx 100\text{meV}$ to be ideally suited. GNR-LNAs with this bandgap, biased at the optimum operating point are ultra-fast (THz) low noise amplifiers exhibiting performance specs that show considerable advantages over state-of-the-art technologies. The optimum operating point and bandgap range is found by simulating the impact of the bandgap on several device and circuit relevant parameters including transconductance, output resistance, band-width, gain, noise figure and temperature fluctuations. Our findings are believed to be of relevance in particular for graphene based RF applications.

Index Terms—Amplifier, Band gap, Graphene, RF, LNA

I. INTRODUCTION

A high performance low noise amplifier is an important building block for radio frequency receiver systems used in modern communication chips for GPS, CDMA, wideband and ultra wideband technologies. State-of-the-art scaled CMOS LNAs⁽¹⁾ exhibit high gain (5-20dB), large bandwidth (BW) (4.5-10GHz), low noise figures (1-2dB), adequate

This work was supported by the Nanotechnology Research Initiative (NRI) through a supplement to the Network for Computational Nanotechnology (NCN), which is supported by National Science Foundation (NSF) under grant number: EEC-0634750.

S.Das and J.Appenzeller are with Electrical and Computer Engineering Department (Birck Nanotechnology Center) at Purdue University, West Lafayette, Indiana 47906. (email : sdas@purdue.edu, appenzeller@purdue.edu). Copyright © 2011 IEEE

linearity and good reliability under all operating conditions. However, further improvements occur possible by the use of novel nano-materials such as graphene⁽²⁾. Here we discuss in detail the importance of creating a small but sizable bandgap in graphene to take full advantage of graphene's superb electrical transport properties.

Graphene, a single layer of graphite, has attracted substantial attention in the scientific research community over the last decade due to its fascinating electrical, chemical, mechanical and optical properties. In particular, high carrier mobilities with the potential to reach ballistic transport conditions, low noise compatibility and high carrier velocities make graphene field-effect transistors (GFETs)^(3,4,5,6) suitable for many applications. Since graphene is a semiconductor with zero bandgap, GFETs show in general poor I_{on}/I_{off} ratio^(7,8). This fact limits the usefulness of graphene for logic applications. While a significant scientific effort aims at creating a bandgap in graphene either by using an electric field⁽⁹⁾ or by forming graphene nano-ribbons⁽¹⁰⁾ or graphene nano mesh⁽¹¹⁾ to overcome this limitation, graphene seems to naturally lend itself to analog applications and especially high performance RF devices like LNAs due to the less stringent demands in terms of off-currents.

What had been ignored as of yet is the detailed impact of Bandgap (E_g) on the voltage Gain(G), Speed or Bandwidth (f_T), Power Dissipation (P), Noise Power (N_s) and Stability (S) of an RF circuit. Under realistic circuit conditions, our findings suggest that neither a zero bandgap nor a gap in the eV range is ideally suited for graphene based RF applications. Instead, we suggest that a bandgap window in the 100meV range allows for optimum small signal circuit performance. This statement also implies that the use of graphene nano-ribbons that exhibit a bandgap due to size quantization occurs not only relevant for logic but also analog applications.

In the following we will provide the logical flow of arguments.

II. IMPORTANT PARAMETERS FOR A LOW NOISE AMPLIFIER

In our evaluation, we use the conventional equations for RF circuit parameters. Moreover, for our considerations we are including the contribution of the so-called quantum capacitance C_q ⁽¹²⁾ that captures the impact of the finite amount of states available in the channel region when evaluating their population for current transport. In addition to intrinsic device parameters, we have included the load impedance g_L and parasitic capacitance contributions C_{par} in our model.

$$f_T = \frac{g_m}{2\pi C_{in}} \quad G = \frac{g_m}{g_L + g_d} \quad (1)$$

$$\frac{dV_{ch}}{dV_{gs}} = \frac{C_{ox}}{C_{ox} + C_q} \quad C_{in} = \frac{C_{ox}C_q}{C_{ox} + C_q} + C_{par} \quad (2)$$

$$C_q = \frac{2}{\pi} \left(\frac{2\pi q}{h\nu_F} \right)^2 WL \frac{\partial}{\partial(qV_{ch})} \int_0^\infty (E - qV_{ch}) (f_s(E, T) + f_d(E - qV_{ds}, T)) dE \quad (3)$$

$$N_S = 2qI_{op}f_T \quad P = V_{op}I_{op} + I_{op}^2/g_L \quad (4)$$

$$S = (1 - F)100\%$$

$$F = \frac{1}{G} \frac{dG}{dT} \Delta T = \frac{1}{g_L + g_d} \frac{dg_d}{dT} \Delta T \quad (5)$$

In equation (1) f_T is the unity current gain⁽¹³⁾, G is the voltage gain⁽¹³⁾. g_m and g_d are the small signal transconductance and output conductance of the GFET respectively. R_G is the lumped gate resistance and g_L an external load conductance that was introduced to avoid an instability in device performance as a function of temperature due to the particular dependence of g_d on temperature as will be explained below. In equation (2), V_{ch} is the channel potential and C_{ox} the gate oxide capacitance. C_{par} captures the impact of parasitic capacitance contributions from the overlap between the gate and the source/drain contacts. In particular, C_{par} is assumed to be proportional to the channel width W as are also C_{ox} and C_q . The reader should note that C_{ox}

and C_q are connected in series while the parasitic capacitance is in parallel. lv_F is the Fermi velocity in graphene - a constant that does not change when varying the charge in the channel. In equation (4), N_s captures the shot noise⁽¹⁴⁾ impact introduced by the amplifier across a 1 ohm resistor due to random electron and hole movement, and P is the power dissipation⁽¹³⁾ in the circuit. I_{op} and V_{op} are the operating current and voltage for the GFET. In equation (5) T is the temperature and S and F denote temperature stability and temperature fluctuation respectively. ΔT is the operating temperature range for the RF device.

III. TOP-DOWN VIEW

In the following we will mainly focus on RF applications where the received signal strength is less than 100 μ V. Examples for applications include satellite and long distance radio communications. The reason for this restriction lies in the I_d - V_{ds} characteristics of GNR-FETs (see Fig.1), which show current saturation only in a very narrow region of the order of the bandgap. We will discuss this topic in greater detail in section V. Moreover, for the above mentioned small signal applications, circuit designers commonly focus on f_T and G which justifies ignoring f_{max} in our analysis.

In order to evaluate the RF performance of a novel device, it is mandatory to compare various parameters as gain (G), speed (f_T), power dissipation (P), noise (N_S) and stability (S) simultaneously, rather than just focusing on one aspect alone. In the following we refer to those parameters as RF surface variables and compare the graphene performance with state-of-the-art values from the literature for benchmarking purposes. As evident from equations (1)-(5), the values of these surface variables depend on g_m , g_d , g_L and the different capacitance contributions. g_m , g_d are determined by the I-V characteristics of the device at the operating point while g_L is an external circuit parameter. The I-V characteristics of the device on the other hand are a result of the band structure of the channel material and hence the bandgap E_g in case of the graphene nano-ribbon transistor. It has been experimentally demonstrated that the band gap of graphene nano-ribbons is inversely proportional to the width of the

ribbon⁽¹⁰⁾ and the empirical relationship found is given by equation (6).

$$E_g = \frac{a}{W \text{ (in nm)}} eV \quad (6)$$

where “a” is a constant. For numerical purposes, we will use $a = 0.8$ ⁽¹⁰⁾. As mentioned earlier all the capacitances are proportional to the channel width W and hence inversely proportional to the band gap E_g . Thus RF surface variables depend on one core variable – E_g – and one external variable – g_L (R_L) – as shown in figure 1. Our aim will be to find the doublet (E_g, g_L) that optimizes the performance of the GNR-FET.

IV. MODEL FOR SIMULATION

Graphene is a two-dimensional sheet of carbon atoms arranged in a hexagonal lattice. It exhibits a linear energy dispersion relationship and linear density of states $D(E)$. To evaluate transport through this material in a three-terminal device geometry, we have calculated the current according to equation (7)⁽¹⁵⁾, assuming ballistic transport conditions and ignoring contact effects that would impact the total transmission probability from source to drain.

$$I = q \int_0^{\max(qV_{gs}, qV_{ds})} D(E)v(E) (f_s(E, T) - f_d(E - qV_{ds}, T)) dE \quad (7)$$

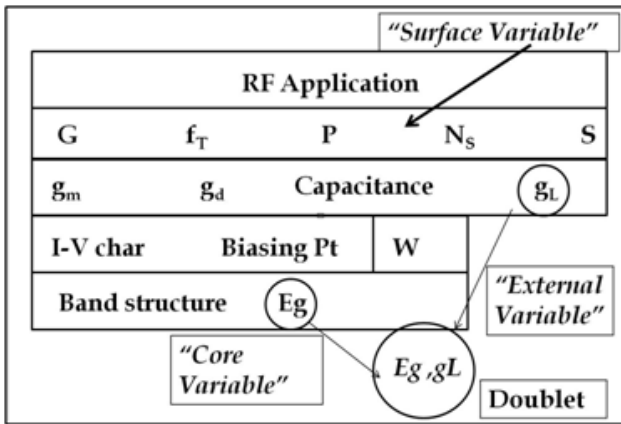


Figure 1. Top-down view of RF-relevant variables.

In this expression $v(E)$ is the carrier velocity and $f_s(E, T)$ and $f_d(E - qV_{ds}, T)$ are the Fermi functions in the source and drain contacts respectively while V_{ch} is the channel potential and V_{ds} is the source to drain potential. The channel length of the simulated device is 50nm and hence it is reasonable to assume that the carrier movement involves no scattering. To get a better intuitive idea of the operation of a graphene nano-ribbon (GNR) transistor, the density of states of this two-dimensional (2D) device can be expressed as the superposition of an appropriate number of one-dimensional (1D) modes with energy spacing between the modes of half the bandgap due to size quantization. Hence the total number of modes contributing to current conduction is directly proportional to the width. In addition, we consider the contributions from direct tunneling across the band gap from source to drain when calculating I according to equation 7. The band-to-band tunneling current contribution was included using WKB⁽¹⁶⁾ approximation.

V. BIASING POINT FOR GNR-FET

The ambipolar nature of the output characteristics of a graphene field-effect transistor shown in figure 2 can be understood in the following way: As long as $V_{ds} < V_{ch}$, the current increases with V_{ds} since new states become available for transport in the channel. However, the increment of current increase with increasing V_{ds} becomes the smaller the closer the Fermi level in drain moves towards the Dirac point (bottom of the conduction band in nano-ribbons) where the density of states vanishes. For $V_{ch} < V_{ds} < E_g + V_{ch}$, the current remains constant. This is the “flat” part of the output characteristics with the smallest g_d value. Please note that this region has a slope of zero only at 0K. At higher temperatures, the Fermi function broadening results in a finite slope instead. Since the broadening is of the order of a few $k_B T$ (k_B being the Boltzmann constant), for graphene devices, which exhibit only a very small or vanishing bandgap, the flat region in figure 2 only extends over a small V_{ds} range, with the smallest slope reached for $V_{ds} = V_{ch}$. For $V_{ds} > E_g + V_{ch}$ the current increases again, with g_d increasing with increasing V_{ds} .

The transconductance g_m shown in the inset of figure 3 on the other hand increases monotonically as long as $V_{ds} < V_{ch}$, before it starts decreasing for $V_{ds} >$

V_{ch} . This means that g_m has a local maxima at $V_{ds} = V_{ch}$ where g_d is minimal. As a result the voltage gain G and the switching speed captured by f_T are maximum at this point. If we assume operation in the quantum capacitance limit (QCL: $C_{ox} \gg C_q$), the case where V_{ch} follows one-to-one the applied gate voltage V_{gs} , the biasing point will be as in equation 8.

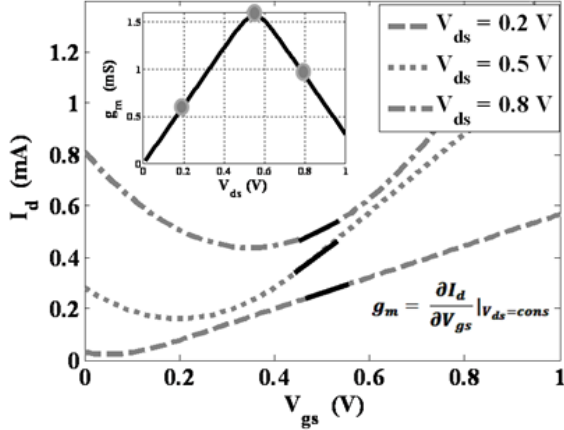


Figure 2. Output characteristics of a single layer graphene nano-ribbon FET at room-temperature ($T=300K$) assuming ballistic transport. The channel length is $L=50nm$, the width is $W=8 nm$ (Bandgap = $100 meV$). Inset shows the variation of output-conductance (g_d) as a function of source to drain voltage with source grounded. The channel potential is kept constant.

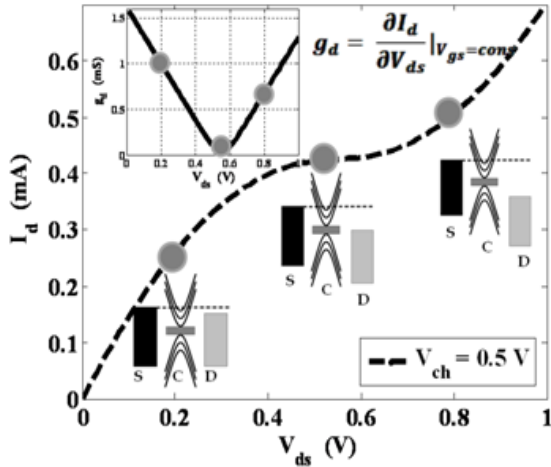


Figure 3. Output characteristics as a function of channel potential. Inset shows the transconductance as a function of source to drain potential at a given gate bias.

$$V_{ds} = V_{gs} = V_{ch} \quad (8a)$$

This will result in optimum device performance. On the other hand, the operating point will be

$$V_{ds} = V_{ch}, \quad V_{gs} = \int_0^{V_{ch}} \left(1 + C_q(V)/C_{ox} \right) dV \quad (8b)$$

if C_q is larger than C_{ox} (classical limit CL).

VI. IMPACT OF BANDGAP ON g_m AND g_d

For the remainder of this discussion we will assume that the GNR-FET is biased at the optimum operating point. We choose $V_{ch}=1V$ in the quantum capacitance limit to allow for a comparison with state-of-the-art LNA circuitry. Furthermore, we used an averaging ac signal strength of $100\mu V$ to ensure linearity in device performance. The main question is how to optimize the performance of this optimally biased GNR-FET by means of a bandgap e.g. associated with a finite nano-ribbon width. For the following discussion we will assume that for zero bias conditions the Fermi levels at the source and drain contact are aligned to the conduction band of the channel. This leads to a slight modification of equation (8a) and (8b):

$$V_{ds} = V_{ch} + E_g/2, \quad V_{gs} = V_{ch} \quad (9a)$$

$$V_{ds} = V_{ch} + E_g/2,$$

$$V_{gs} = \int_0^{V_{ch}} \left(1 + C_q(V)/C_{ox} \right) dV \quad (9b)$$

A first order small signal circuit model for an FET has only two device parameters g_m and g_d . As the transconductance g_m is directly proportional to the number of conducting modes and the number of conducting modes is directly proportional to the width of the graphene nano-ribbon and W is proportional to $1/E_g$ according to eq. (6), we obtain:

$$g_m \propto W \propto 1/E_g \quad (10)$$

The inset of figure 4 shows the dependence of g_m/W as a function of W . It is interesting to note that for a given channel potential there is a critical width (W_c) below which equation 10 does not hold true anymore. For small W the mode spacing becomes extremely large and the nano-ribbon becomes truly 1-D in the sense that only *one* 1-D mode contributes to the current flow for a given channel potential. This implies that g_m becomes constant and thus g_m/W increases with decreasing W . However if we increase the channel potential, then for single mode operation the mode spacing would have to be much higher to ensure 1-D transport, which explains the smaller critical width. For a channel potential ($V_{ch}=1V$) the critical thickness is 0.9nm. Throughout the remainder of this paper we will be using much larger W values which justifies the use of equation 10.

In general, devices that show current saturation over a wide V_{ds} -range in their output characteristics exhibit an output conductance g_d close to zero. Current saturation in these devices is a manifestation of either the impact of the bandgap or scattering (or both). Since scattering effects are absent in ballistic devices, the bandgap alone is responsible for the saturation region. Hence, for ballistic graphene nano-ribbons, current saturation occurs over a voltage range of the order of the bandgap with a finite value of g_d at non-zero temperatures. As the bandgap increases, g_d decreases towards zero. The empirical relationship between bandgap and g_d is given by equation (11).

$$g_d = \frac{\alpha(T)}{E_g^{1.5+0.001(T-300)}} \quad (11)$$

where $\alpha(T)$ is a constant that depends very weakly on temperature. Note that the expression for g_d is a fit.

VII. IMPACT OF BANDGAP ON SURFACE VARIABLES

The most relevant circuit parameters for radio frequency analog application are speed or bandwidth (f_T), gain (G_{\square}), noise power (N_s) and temperature stability (S). It is important to recall that all the capacitance contributions used in equation (2) and (3) are proportional to the width of the nano ribbon and thus inversely proportional to the bandgap. This

implies that any capacitance contribution per unit width is independent of E_g . Hence f_T , which is directly proportional to g_m and inversely proportional

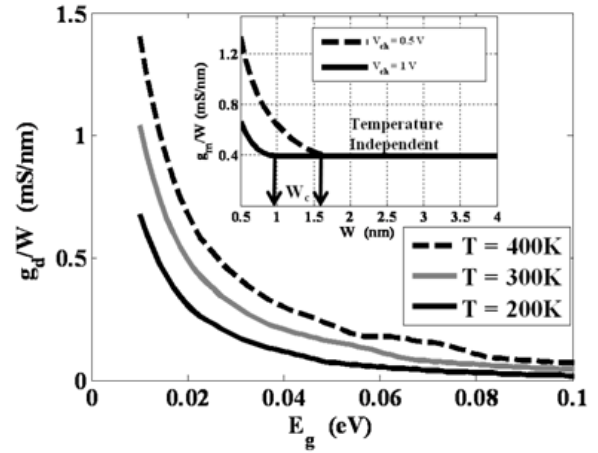


Figure 4. Dependence of output conductance per unit width on the size of the bandgap at different temperatures. The inset shows the dependence of transconductance per unit width on ribbon width(bandgap).

to the input capacitance is also constant (see equation 12). The magnitude of f_T depends on whether the device is dominated by parasitic or intrinsic capacitance components. Assuming a reasonable C_{par} value of $100fF/\mu m^2$, an f_T of around 8 THz can be calculated for a 50nm channel length device. γ and β are constants, independent of band gap.

$$f_T = \frac{g_m}{2\pi C_{in}} = \frac{\gamma/E_g}{2\pi \beta/E_g} = \frac{\gamma}{2\pi\beta} \quad (12)$$

An amplifier in general adds noise to the output signal. Since the GNR-FET discussed here shows a large bandwidth in the THz range, one may not neglect the shot noise introduced by the device. The shot noise power is directly proportional to the product of bandwidth and operating current as described in equation (4). The usual way to evaluate the level of noise in an amplifier is the noise figure (NF) defined as the ratio of the signal to noise ratio (SNR) between the input and the output of the amplifier. The noise figure simulated for a GFET at the fixed operating point is constant as a function of bandgap as the bandwidth f_T is constant. For 50nm intrinsic devices operating at 1V (corresponds to a

current of around 10mA) the noise figure corresponding to a 10nW input noise is 1.6dB.

Low Noise amplifiers often have to operate under temperatures conditions that can easily span a range from -70°C to +150°C. This requires that LNAs exhibit considerable stability under these conditions. Since the bandgap of graphene for not too aggressively scaled nano-ribbons is at best of the order of $k_B T$ at room-temperature, the impact of temperature needs to be carefully evaluated. Since the number of conducting one-dimensional modes itself does not depend on T - although the population of the modes of course does - g_m is almost independent of temperature. However g_d increases with temperature as the slope of the plateau in the I_d - V_{ds} characteristics close to the operating point increases with temperature. Obviously, this effect is more pronounced for smaller bandgaps that show a smaller plateau region. This is also evident from figure 4. Thus it is clear that f_T remains unaffected by temperature over the operating temperature range while the voltage gain is expected to sensitively depend on temperature variations due to its g_d - dependence. Rewriting equation (5), we obtain:

$$F = \frac{1}{g_L + g_d} \frac{dg_d}{dT} \Delta T = \frac{g_d(T_{450K}) - g_d(T_{200K})}{g_d(T_{300K}) + g_L} \quad (13)$$

Figure 5 displays how the above defined temperature fluctuation amplitude F changes as a function of bandgap for different load resistances. Since a larger bandgap results in an output conductance that is constant over a wider voltage range, temperature fluctuations are less pronounced in this case. From this perspective the larger the bandgap the better the stability ($S=1-F$). However it is important to note, that the same stability value can be obtained when using a smaller bandgap in combination with a larger load conductance (smaller load resistance).

Since at the operating point the output conductance is much smaller than the load conductance, the equation for gain G can be rewritten as:

$$G = \frac{g_m}{g_d + g_L} = \frac{\gamma/E_g}{g_L} = \frac{\gamma}{g_L E_g} \quad (14)$$

It is obvious from this equation that a smaller load conductance (larger load resistance) and smaller bandgap are both essential for higher gain. Table 1 summarizes all of the above findings, indicating the desired trends in terms of E_g and g_L to improve the different surface variables.

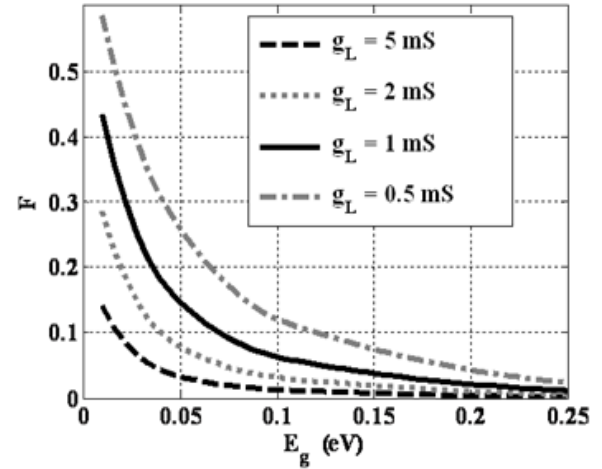


Figure 5. Fluctuation amplitude F as a function of bandgap for different load conductance values g_L .

TABLE 1

	E_g	$g_L(R_L)$
<i>Speed(f_T)</i>	<i>No Dependence</i>	<i>No Dependence</i>
<i>Noise figure(N_S)</i>	<i>No Dependence</i>	<i>No Dependence</i>
<i>Gain(G)</i>	<i>Small</i>	<i>Small (Large)</i>
<i>Stability (S)</i>	<i>Large</i>	<i>Large (Small)</i>

VIII. Optimizing Performance

From the above discussion it is clear that the two most important parameters are the gain and stability and that they show exactly the opposite trends as a function of bandgap. Having no bandgap gives maximum gain at the cost of minimum stability while having infinite bandgap gives maximum stability and no gain. Stability and gain also depend upon the choice of load resistance. A smaller load resistance results in a smaller gain but larger stability while a larger load resistance has the opposite effect.

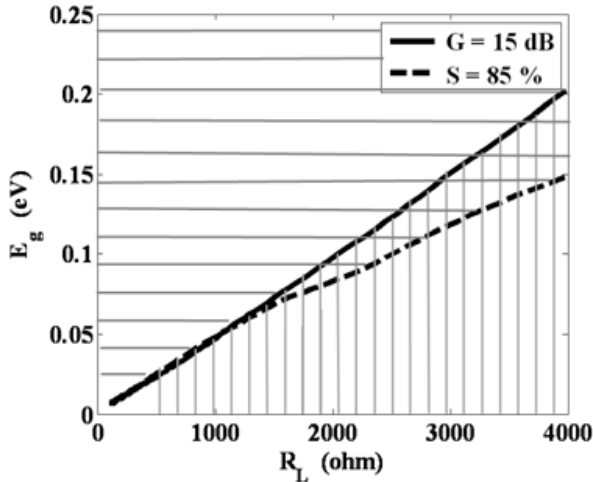


Figure 6. Constant stability and constant gain contours.

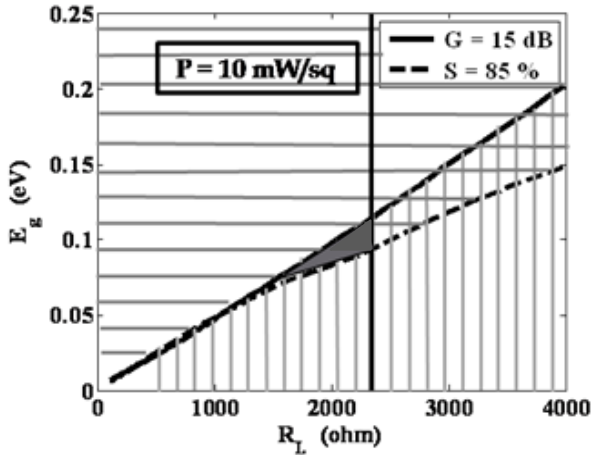


Figure 7. Constant stability, Constant gain, Constant Power Dissipation contours.

The question to address next is thus: “What is the ideal pair (doublet) of bandgap and load resistance (E_g, R_L) that allows for the desired LNA performance?”

As apparent from figure 5, for a given choice of F (and thus S), multiple doublets (E_g, R_L) are obtained. Similarly, from equation (15), we can easily deduce another set of doublets that results in a constant G -value.

Figure 6 displays constant stability and constant gain contours. Any doublet in the space above the constant stability contour and below the

constant gain contour satisfies the demands in terms of S and G – here G better 15dB and S better 85%. It is apparent from figure 6 that utilizing a larger bandgap and higher load resistance value improves the likelihood of satisfying the S and G requirement. However, one more constrain that sets an upper limit for the doublet has not been considered so far, i.e. the amount of power dissipation given by equation (4).

Power dissipation contours are vertical straight lines as shown in figure 7, and any power constraint implies that only (E_g, R_L) doublets left of this line are allowed solutions. The shaded region represents the (E_g, R_L) doublets that satisfy stability $> S$, gain $> G$ and power dissipation $< P$. For different combinations of the triplet [S, G, P] one obtains different shaded regions and the values of this triplet depend upon the particular type of application and its requirements. For present state of art LNA applications a triplet [$S=85\%, G=15\text{dB}, P=10\text{mW/sq}$] represents a reasonable choice. Under these conditions, a load resistance of $2\text{k}\Omega$ ⁽¹⁸⁾ and a non-vanishing bandgap in the range of $80\text{-}100\text{meV}$ ⁽¹⁹⁾ are solutions that satisfy the above conditions.

IX. CONCLUSION

In summary, we have analyzed the impact of the bandgap in graphene nano-ribbons on the RF-performance of GNR-FETs. We find that there exists an optimum bandgap choice when considering stability S , gain G and power dissipation P simultaneously. If a graphene nano-ribbon device is designed and fabricated in such a way that its bandgap and load conductance belong to the intersection set [i] and it is biased at the recommended operating point, it is expected to satisfy the [S, G, P] requirement along with ultra fast speed and at a low noise level.

* The reader may argue that there is no Schottky barrier for a sheet of graphene as it has zero bandgap. However, due to size quantization in a GNR, each 1-D mode with its associated band structure represents its own Schottky barrier device. This effect has been ignored in our model and we have assumed 100% source and drain injection probability instead for any given Fermi energy.

ACKNOWLEDGEMENT

This work was supported by the Nanotechnology Research Initiative (NRI) through a supplement to the Network for Computational Nanotechnology (NCN), which is supported by National Science Foundation (NSF) under grant number: EEC-0634750.

REFERENCES

- [1]. Hakan Kuntman et al., Analog Integrated Circuit Signal Process, vol. 60, page 169–193 (2009)
- [2]. Geim, A. K. et al., Nature Materials, vol. 6, page 183–191 (2007)
- [3]. P.R.Wallace et al., Physical Review, vol. 71, page 622–634 (1947)
- [4]. Sandip Niyogi et al., J. Am. Chem. Soc, vol. 128 (24), page 7720–7721 (2006)
- [5]. C. Lee et al., Science, vol.321 (5887), page 385–388 (2008)
- [6]. Y.Zhang et al., Nature, vol.459 (7248), page 820–823 (2009)
- [7]. Y. Q. Wu et al., Applied Physics Letter, vol. 92, 092102 (2008)
- [8]. Lemme, M. C. et al., IEEE Electron Device Letters, vol.28, page 282–284 (2007).
- [9]. K.F.Mak et al., Physical Review Letter, vol.102, page 256405 (2009)
- [10]. P.Kim et al., Physical Review Letter, vol. 98, page 206805 (2007)
- [11]. J.Bai et al., Nature Nanotechnology, vol 5, page 190 (2010)
- [12]. Z. Chen and J. Appenzeller, IEDM Technical Digest , page 509 (2008)
- [13].Microelectronic Circuits, Fourth Edition, Sedra and Smith, Oxford University Press, 1998.
- [14].Modern Digital and Analog Communication System , Third Edition, B.P.Lathi, Oxford University Press, 1998.
- [15].Landauer et al., IBM J. Res Dev, vol 32, page 306 (1988)
- [16].Introduction to Quantum Mechanics, Griffiths, 2nd Edition, Prentice Hall, 2004
- [17].The device on/off current ratio is 15 for a graphene nano-ribbon width of 8 nm corresponding to a band gap of 100 meV. But this aspect is not important for the type of application being investigated here.
- [18]. The reader might question the requirement of a high load impedance ($2k\Omega$) since most RF applications are taking place in a 50Ω environment. Note, that a matching network is in general essential to enable a graphene based nano-circuit. However, a detailed analysis of this topic is outside the scope of this paper.



Saptarshi Das was born in Kolkata, India in 1986. He received his BS degree from Jadavpur University, India. He is currently pursuing his PhD degree in Electrical Engineering from Purdue University, USA.

In the summer of 2009 he worked as an intern at IBM T.J.Watson Research Center, Yorktown. His research focuses on device and circuit modeling and optimization of novel nano transistors for RF application. He also works on the experimental realization of ferroelectric low power transistors.



Joerg Appenzeller (M'02–SM'04–F'10) received the M.S. and Ph.D. degrees in physics from the Technical University of Aachen, Aachen, Germany, in 1991 and 1995, respectively. His Ph.D. dissertation investigated quantum transport in low-dimensional systems based on III/V heterostructures.

He worked for one year as a Research Scientist with the Research Center, Juelich, Germany, before he became an Assistant Professor with the Technical University of Aachen, in 1996, working on electronic transport in carbon nanotubes and superconductor–semiconductor hybrids. From 1998 to 1999, he was with the Massachusetts Institute of Technology, Cambridge, as a Visiting Scientist, exploring the scaling limits of Si-MOSFETs. From 2001 to 2007, he was with the IBM T.J. Watson Research Center, Yorktown, NY, as a Research Staff Member, where he was mainly involved in the investigation of carbon nanotubes and silicon nanowires for future nanoelectronics. Since 2007, he is a Professor of Electrical and Computer Engineering with Purdue University, West Lafayette, IN, and Scientific Director of Nanoelectronics with the Birck Nanotechnology Center. His current interests include novel devices based on nanomaterials such as nanowires, nanotubes, and graphene.